NIH Public Access
Author Manuscript
Polymer (Guildf). Author manuscript; available in PMC 2016 February 10.

Published in final edited form as:
Polymer (Guildf). 2015 February 10; 58: 30–35. doi:10.1016/j.polymer.2014.12.031.

A Fluidic Device with Polymeric Textured Ratchets

Koray Sekeroglu and **Melik C. Demirel***
Materials Research Institute and Department of Engineering Science and Mechanics, Pennsylvania State University, University Park, Pennsylvania 16802, USA

Abstract

Nanotextured surfaces are widely used throughout nature for adhesion, wetting, and transport. Chemistry, geometry, and morphology are important factors for creating tunable textured surfaces, in which directionality of droplets can be controlled. Here, we fabricated nano textured polymeric surfaces, and studied the effect of tilting on the mobility of frequency modulated water droplet transported on asymmetric nano-PPX tracks. Plastically-deformed tracks guided water droplets for sorting, gating, and merging them as a function on their volume. Polymeric ratchets open up new avenues for the fields of digital fluidics and flexible device fabrication.

INTRODUCTION

Textured surfaces composed of nanoscale structures are widely used throughout nature for adhesion, wetting, and transport.[1–7] Inspired by natural surfaces [8, 9], a myriad of synthetic surfaces [10] with precisely tuned physicochemical properties to these functions were fabricated. Ranging from templated and template-free deposition to photolithography to direct printing, numerous techniques for manufacturing textured surfaces have been developed. For example, a micro-scale smooth surface enables transporting droplets, micro-scale pumps, and adhesion [11]. Recently, bio-derived thermoplastics have also been used for fabrication of textured surfaces.[12]

Directional droplet motion on engineered surfaces have been extensively investigated via capillary action [13], electrowetting [14], focused acoustic waves [15], surface tension [16], transistor based actuation [17], Leidenfrost ratchets [18], and chemical gradient [19]. For example, droplets flow unidirectionally on asymmetrical surfaces due to vibrational frequency. Additionally, Sandre *et al*.[20], created directional micro-ratchets that are parallel, permitting water droplet transport using a breathing motion [20]. Likewise, Linke *et al*., investigated the propulsion of water droplets on micro-ratcheted surfaces at a

© 2014 Elsevier Ltd. All rights reserved.

*Author to whom correspondence should be addressed. Phone: 1-814-863-2270, mdemirel@engr.psu.edu.

Publisher's Disclaimer: This is a PDF file of an unedited manuscript that has been accepted for publication. As a service to our customers we are providing this early version of the manuscript. The manuscript will undergo copyediting, typesetting, and review of the resulting proof before it is published in its final citable form. Please note that during the production process errors may be discovered which could affect the content, and all legal disclaimers that apply to the journal pertain.

AUTHOR CONTRIBUTIONS

MCD planned, developed, and supervised the research. KS worked on the device fabrication and wetting measurements under the guidance of MCD. All authors contributed to writing and revising the manuscript, and agreed on its final contents.

NIH-PA Author Manuscript
NIH-PA Author Manuscript
NIH-PA Author Manuscript

NIH-PA Author Manuscript

NIH-PA Author Manuscript

NIH-PA Author Manuscript

Leidenfrost state, concluding that the directional movement of the water droplets occurred due to vapor flow between a liquid (i.e., boiling water) and a solid surface (i.e., anisotropic ratchets) [21]. Shastry *et al*., produced microstructures with a superhydrophobic gradient, which propelled water droplets upon application of a mechanical vibration [22].

Surface chemistry, geometry, and morphology are important factors for creating tunable ratchets, in which directionality of droplets can be controlled. Recent work of tunable ratchets includes work of Bohringer and coworkers [23] who propelled droplets along a horizontal surface as well as studying the role of curvature for ratcheting performance.[24] Leidenfrost temperature-dependent tunable ratchets [25] as well as oil-based rachets were also recently fabricated including a directional oil-sliding, micro-grooved surface that combines omniphobic and anisotropic sliding [26]. Another parameter for tunable ratchets is the effect of contact angle hysteresis on the motion of drops subjected to an asymmetric vibration [27]. Additionally, chemical asymmetry has also been demonstrated to control reversible and unidirectional liquid transport by virtue of triangular micro-prisms consisting of thermo-responsive polymers.[28]

To date, simple platforms have been built to introduce assembly lines at micro-scale including devices, which not only carry micro-sized cargo, but also specify targets (e.g., directed assembly of microgels by microliter droplets via water transport across textured surfaces). Daniel *et al*., [29] and Mettu *et al*., [30], for instance, displayed that water droplets on non-wetting flat surfaces can be guided directionally by vibrating the surface asymmetrically. Meanwhile, our group fabricated nanotextured surfaces that can transport microliter water droplets unidirectionally via vertical vibrations [31], and Duncombe *et al*., engineered a surface with directional tracks to transport droplets on circular pathways [32]. These successful applications of directional water transport for micro-assembly, however, bring new challenges towards optimizing micro-assembly platforms to the forefront [32].

New strategies for merging and sorting droplets on directional pathways as well as a rapid addition of desired paths are essential for improvements in micro-assembly. To that end, we focused on wetting hysteresis that could be varied by controlling the texture geometry [33] (e.g., spacing, density, and angle of asymmetry) of oblique angle deposited polymers. Previously, upon moving water droplets unidirectionally across a polymeric nanotextured surface, [34] we reported that water droplets on a nanotextured surface could be leveraged as a soft cargo carrier. Furthermore, we demonstrated that the velocity of the droplet transport depends on the frequency of vertical vibrations and the droplet volume [35]. Here, we studied the effect of tilting on the mobility of frequency modulated water droplet transported on asymmetric textured surfaces with tracks fabricated by adjusting the asymmetric orientation (i.e., angle of anisotropy) of the nanotextured surface. As a result, we demonstrated sorting and merging of water droplets, thereby enhancing potential for the fields of digital fluidics and device fabrication.

RESULTS

We fabricated asymmetric textured surfaces via oblique angle polymerization of poly(p-xylylene), commercially known as Parylene [36]. In this process, monomer vapors produced

NIH-PA Author Manuscript

NIH-PA Author Manuscript

NIH-PA Author Manuscript

by pyrolysis of chemically functionalized *p-chloro-xylylene* precursors are directed at an oblique angle of ten degrees towards a substrate to initiate textured polymer growth. This inclined deposition induces growth of textured Parylene or nano-PPX, a nanostructured surface comprised of clusters of submicron diameter nano-rods. Nano-PPX is a flexible polymer that has a Young's Modulus of 100 MPa [11]. With hydrophobic surfaces (static contact angle ≥ 90°) and apparent water contact angles as high as 120°, the nano-PPX's surface could be plastically deformed under constant pressure to create tracks. Figure 1a shows deformation of the nano-PPX surface under constant pressure along the nano-rod direction using a rubber strip. Cross sectional electron images demonstrate the effect of pressure for pristine and deformed surfaces in Figure 1b and 1c respectively. Figure 1d shows guided transport of a 5 μL droplet on the deformed nano-PPX surface, which performed on the deformed track with a constant velocity of 11.5 mm/s following a straight path. Figure 1e shows a control experiment that tested water transport performance by droplets on planar- and nano-PPX surfaces. Straight tracks were fabricated on both nano-PPX and planar-PPX coated surfaces with 5 μl droplets placed on each. Mechanical vibrations were applied and set to a frequency of 95 Hz at an approximate 0.5 mm amplitude. The water droplet on the nano-PPX surface moved unidirectionally on the track whereas the droplet on the planar-PPX surface was sessile.

Nano-PPX films were further characterized by their capacity as a micro-assembly platform to transport and sort water droplets. To that end, we studied their anisotropic wetting behavior as well as associated droplet transport rates both via track formation and under variable surface pressures. Finally, we developed methods of sorting, mixing, and guiding droplets on nano-PPX.

Nano-PPX, composed of an array of nano-rods, provides a smooth nano-film on which to transport microliter droplets and, thus, demonstrates anisotropic wetting behavior by means of a pin-release droplet ratchet mechanism. Anisotropic wetting property of nano-PPX can be quantified by the critical droplet volume (***V***), the maximum water droplet volume adhering on the surface at an angle α. Critical droplet volume is reached when the gravitational force is equal to the retention force on the droplet. Figure 2a represents the ***V*** values for various stage angles ($65° < \alpha < 90°$) at pinning, release, and isotropic (+ and −) directions. It shows that critical drop volumes for the release directions are larger than the pinning and isotropic directions and that isotropic (+) and isotropic (−) exhibit similar critical droplet volume at specific angles due to a lack of hysteresis along the isotropic direction. The ratio of critical drop volume in pinning direction to release direction is expressed as $V_{PIN} = C_0 \bullet V_{REL}$, where $\mathbf{C_0}$, a constant, is the strength of wetting anisotropy on the nano-PPX surface. Figure 2b shows that $\mathbf{C_0}$ for the anisotropic axis ranges from 0.75 to 0.85. Adversely, $\mathbf{C_0}$ for the isotropic axis revolves around 1.0; hence, implying negligible wetting anisotropy. Figure 2c demonstrates the inverse relationship between the frequency of vibration and water droplet size on the deformed nano-PPX surface as water droplets are transported on the nano-PPX surface via vibrational frequencies at low amplitude (i.e., 0.5mm). This is explained by Rayleigh's spherical volumes theory and can be quantified as $\omega = \sqrt{(8\gamma/3\pi m)}$, where ω is the frequency of vibration, γ is water surface tension, and ρ is water density. Figure 2d shows the droplet speeds as a function of normalized vibrational

NIH-PA Author Manuscript

NIH-PA Author Manuscript

NIH-PA Author Manuscript

frequencies such that $\omega^* = \sqrt{(\gamma/m)}$, where **m** is droplet mass, and ω^* is the natural frequency. The curves, for drop speeds, overlap even though the data was collected at different frequencies. Overlapping is due to the Rayleigh scaling of natural frequencies.

Next, we investigated the droplet velocity related to the tilt angle of nano-PPX films, discovering that the growth of nano-rods is anisotropic when at a 45 degree angle from the substrate plane. By varying the tilting angle and increasing the normal pressure on the surface, however, the bending of the nano-PPX rods increases and the nano-rod spacing decreases. Figure 3a shows the cross section and top view image (inset) of the nano-PPX rods deposited on a glass substrate. Figure 3b–d show the cross sectional and top view of nano-PPX films with b, c, and d corresponding with angles θ equal respectively to 32°, 24°, and 20° and Figure 3e depicts the increasing pressures on these surfaces, thereby confirming that the tilt angle of the nanorods is inversely proportional to the applied pressure. Moreover, as the nanorods were compacted under increasing pressure, the surface porosity decreased. We tested velocity of various droplet volumes (between 4 to 8 μL) on the tilted nano-PPX surfaces as a function of tilt angles (i.e., θ = 45°, 32°, 24°, 20°). Due to the decreased porosity, the droplet speed is higher on deformed surfaces compared to pristine nano-PPX (45°). Among the tilted surfaces, 24° and 32° angles exhibited higher velocity compared to 20° tilt angle. Most likely, this is due to increase roughness and loss of nano-texture (Figure 3).

We introduced a method of track fabrication to study the effect of channel width on drop speed. This was achieved by using a soft pen with a silicone tip attached to an electronic device controlled by an XY motorized stage as shown in Figure 4a. The pen's tip diameter determines the channel width. Figure 4b shows the top view image of the tracking edge. When the water droplet was placed on a track smaller than itself, it was in contact with both nano-PPX and deformed nano-PPX. Therefore, it was essential to investigate how the track width of the deformed nano-PPX affected the droplet speed on the surface. Figure 4c illustrates the relationship between the droplet speed and the track width of deformed nano-PPX with a fixed droplet size where if the track width is increased, the water droplets move faster on the surface. Reaching 16mm/s at maximum width (i.e., w=2r), the droplets move four times faster on the deformed nano-PPX surface.

Finally, studying droplet size, we designed simple devices (e.g., sorter, mixer, and gate) to guide and assemble droplets on the nano-PPX surface. Figure 5a–b demonstrates a volume-dependent sorting device. A water droplet of 0.8 μl in volume was placed on Track 1 (Figure 5a). This droplet was transported along Track 1 without switching to other tracks on the surface. A larger drop of 5 μl in volume, on the other hand, (Figure 5b) switches to Tracks 2 and 3, which provides the volume dependent sorting. Noting the contour line diameter of droplets, we observed that when the drop diameter is smaller than the track width, the water droplets remain in Track 1. If the drop diameter is larger than the sum of the track width and the distances between the tracks, however, the water droplet switches to the second track. Figure 5c–d demonstrates a volume-dependent mixing device. In Figure 5c, two 2 μl droplets were placed respectively on Tracks 1 and 3 and transported on them from the beginning to the end without any mixing. Depicted in Figure 5d, larger (4 μl) droplets were placed on Tracks 1 and 3. Both droplets moved independently until they approached the

NIH-PA Author Manuscript

NIH-PA Author Manuscript

NIH-PA Author Manuscript

junction at Track 2 where they converge to form the 8 μl which is then transported to the end of the device. Figure 5e diagrams a discriminating ‘gate’ design, in which two parallel tracks (i.e., one continuous and other instead discontinuous) were fabricated. The discontinuous track only enables transport of droplets of sufficient volume that bridge the gap in the second track. Thus, the water droplet transport becomes volume dependent. For example, although a 2 μl droplet could not proceed beyond the gate, by incrementally (i.e., 2 μl increases) changing the volume, we showed that once a 10 μl volume was achieved, unidirectional water transport to the termination of the track was permitted by propulsion due to vibration frequencies.

CONCLUSION

We fabricated nano-PPX surfaces and studied the effect of tilting on the mobility of frequency modulated water droplet transported on asymmetric nano-PPX tracks. Plastically-deformed tracks guided water droplets for sorting, gating, and merging them as a function on their volume. Droplet speeds were measured between 5 to 30 mm/s, which is ideal for transport in digital fluidic devices. The sorter device was used to separate two droplets based on volume, whereas the mixer device merged droplets as a function of volume and the gate device required a threshold volume for droplet transport.

Our future work will continue on nano-PPX but focus on the transportation of (non-water) organic liquids. In addition to surface energy modifications, adjusting the nano-rod arrangement in terms of the nano-rods’ lateral and longitudinal spacing [37] as well as encapsulating surfactants in between nano-rods could provide oleophobic transport.

ACKNOWLEDGEMENT

The authors gratefully acknowledge financial support for this work from the National Institutes of Health (R21HL112114-01) and the Pennsylvania State University.

REFERENCES

1. Ybert C, Barentin C, Cottin-Bizonne C, Joseph P, Bocquet L. Physics of Fluids. 2007; 19:123601.
2. Davis AMJ, Lauga E. Phys. Fluids. 2009; 21(11):113101.
3. Davis AMJ, Lauga E. Journal of Fluid Mechanics. 2010; 661(1):402–411.
4. Bocquet L, Barrat J-L. Soft Matter. 2007; 3(6):685–693.
5. Lauga, E.; Brenner, MP.; Stone, HA. Microfluidics: The no-slip boundary condition. In: Tropea, C.; Yarin, A.; Foss, JF., editors. Handbook of Experimental Fluid Dynamics. New York: Springer; 2007. p. 1219-1240.
6. Rothstein JP. Annual Review of Fluid Mechanics. 2010; 42:89–109.
7. McHale G, Newton MI, Shirtcliffe NJ. Soft Matter. 2010; 6(4):714–719.
8. Bush JWM, Hu DL. Annu. Rev. Fluid Mech. 2006; 38:339–369.
9. Hsu S-H, Woan K, Sigmund W. Mat. Sci. Eng. R. 2011; 72(10):189–201.
10. Kwak MK, Jeong H-E, Kim T-I, Yoon H, Suh KY. Soft Matter. 2010; 6(9):1849–1857.
11. So E, Demirel MC, Wahl KJ. Journal of Physics D: Applied Physics. 2010; 43(4):045403.
12. Pena-Francesch A, Florez S, Jung H, Sebastian A, Albert I, Curtis W, Demirel MC. Advanced Functional Materials. 2014 in press.
13. Ahmadi A, Devlin KD, Najjaran H, Holzman JF, Hoorfar M. Lab on a chip. 2010; 10:1429. [PubMed: 20480107]

NIH-PA Author Manuscript

NIH-PA Author Manuscript

NIH-PA Author Manuscript

14. Pollack MG, Shenderov AD, Fair RB. Lab Chip. 2002; 2:96–101. [PubMed: 15100841]
15. Demirci U, Montesano G. Lab Chip. 2007; 7:1139–1145. [PubMed: 17713612]
16. Berthier E, Beebe DJ. Lab on a chip. 2007; 7:1475. [PubMed: 17960274]
17. Perl A, Gomez-Casado A, Thompson D, Dam HH, Jonkheijm P, Reinhoudt DN, Huskens J. Nature Chemisty. 2011; 3:317–322.
18. Lagubeau G, Le Merrer M, Clanet C, Quéré D. Nature Physics. 2011; 7:395–398.
19. Chaudhury MK, Whitesides GM. Science. 1992; 256:1539–1541. [PubMed: 17836321]
20. Sandre O, Gorre-Talini L, Ajdari A, Prost J, Silberzan P. Physical Review E. 1999; 60:2964–2972.
21. Linke H, Alemán BJ, Melling LD, Taormina MJ, Francis MJ, Dow-Hygelund CC, Narayanan V, Taylor RP, Stout A. Physical Review Letters. 2006; 96:154502. [PubMed: 16712160]
22. Shastry A, Case MJ, Böhringer KF. Langmuir. 2006; 22:6161–6167. [PubMed: 16800671]
23. Duncombe TA, Erdem EY, Shastry A, Baskaran R, Böhringer KF. Advanced Materials. 2012; 24(12):1545–1550. [PubMed: 22331660]
24. Duncombe TA, Parsons JF, Böhringer KF. Langmuir. 2012; 28(38):13765–13770. [PubMed: 22934529]
25. Grounds A, Still R, Takashina K. Scientific reports. 2012; 720
26. Kang SM, Lee C, Kim HN, Lee BJ, Lee JE, Kwak MK, Suh KY. Advanced Materials. 2013; 25(40):5756–5761. [PubMed: 23913781]
27. Daniel S, Chaudhury MK. Langmuir. 2002; 18(9):3404–3407.
28. Kim SM, Koh JH, Suh HS, Yoon H, Suh K-Y, Char K. Soft Matter. 2013; 9(16):4145–4149.
29. Daniel S, Chaudhury MK, de Gennes PG. Langmuir. 2005; 21:4240–4248. [PubMed: 15836001]
30. Mettu S, Chaudhury MK. Langmuir. 2011; 27:10327–10333. [PubMed: 21728326]
31. Malvadkar NA, Hancock MJ, Sekeroglu K, Dressick WJ, Demirel MC. Nature Materials. 2010; 9:1023–1028.
32. Duncombe TA, Erdem EY, Shastry A, Baskaran R, Boehringer KF. Advanced Materials. 2012; 24:1545–1550. [PubMed: 22331660]
33. Extrand C. Langmuir. 2007; 23(4):1867–1871. [PubMed: 17279668]
34. Malvadkar NA, Hancock MJ, Sekeroglu K, Dressick WJ, Demirel MC. Nature materials. 2010; 9(12):1023–1028.
35. Sekeroglu, K. Applications of Asymmetric Nanotextured Parylene Surface Using Its Wetting and Transport Properties. The Pennsylvania State University; 2013.
36. Cetinkaya M, Malvadkar N, Demirel MC. Journal of Polymer Science Part B-Polymer Physics. 2008; 46:640–648.
37. Demirel G, Malvadkar N, Demirel MC. Thin Solid Films. 2010; 518(15):4252–4255.

NIH-PA Author Manuscript
NIH-PA Author Manuscript
NIH-PA Author Manuscript

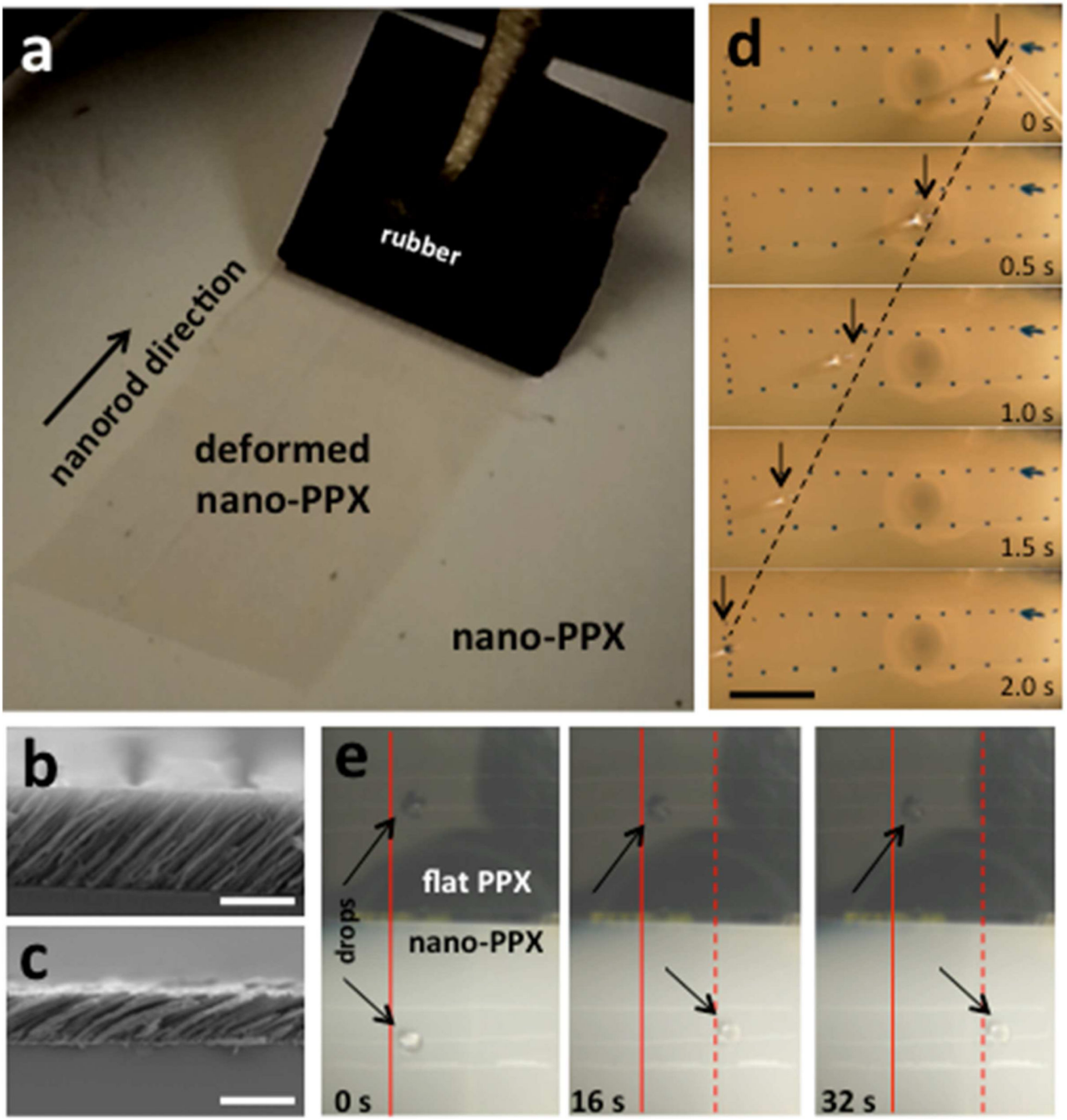

Figure 1.

(a) Nano-PPX surface is deformed by a rubber strip along the nano-rod direction (scale: 1mm). (b) Cross sectional SEM of nano-PPX before (scale: 10μm) and (c) after (scale: 5μm) deformation are shown. (d) Motion of a 5 μL water droplet on the deformed nano-PPX surface at a vibrational frequency of 95 Hz (Scale: 1cm). Dots show the deformed part of the surface. Straight lines indicate constant velocity of the droplet. (e) Droplet moves unidirectionally on the nano-PPX surface, but it is sessile on the planar PPX track.

NIH-PA Author Manuscript
NIH-PA Author Manuscript
NIH-PA Author Manuscript

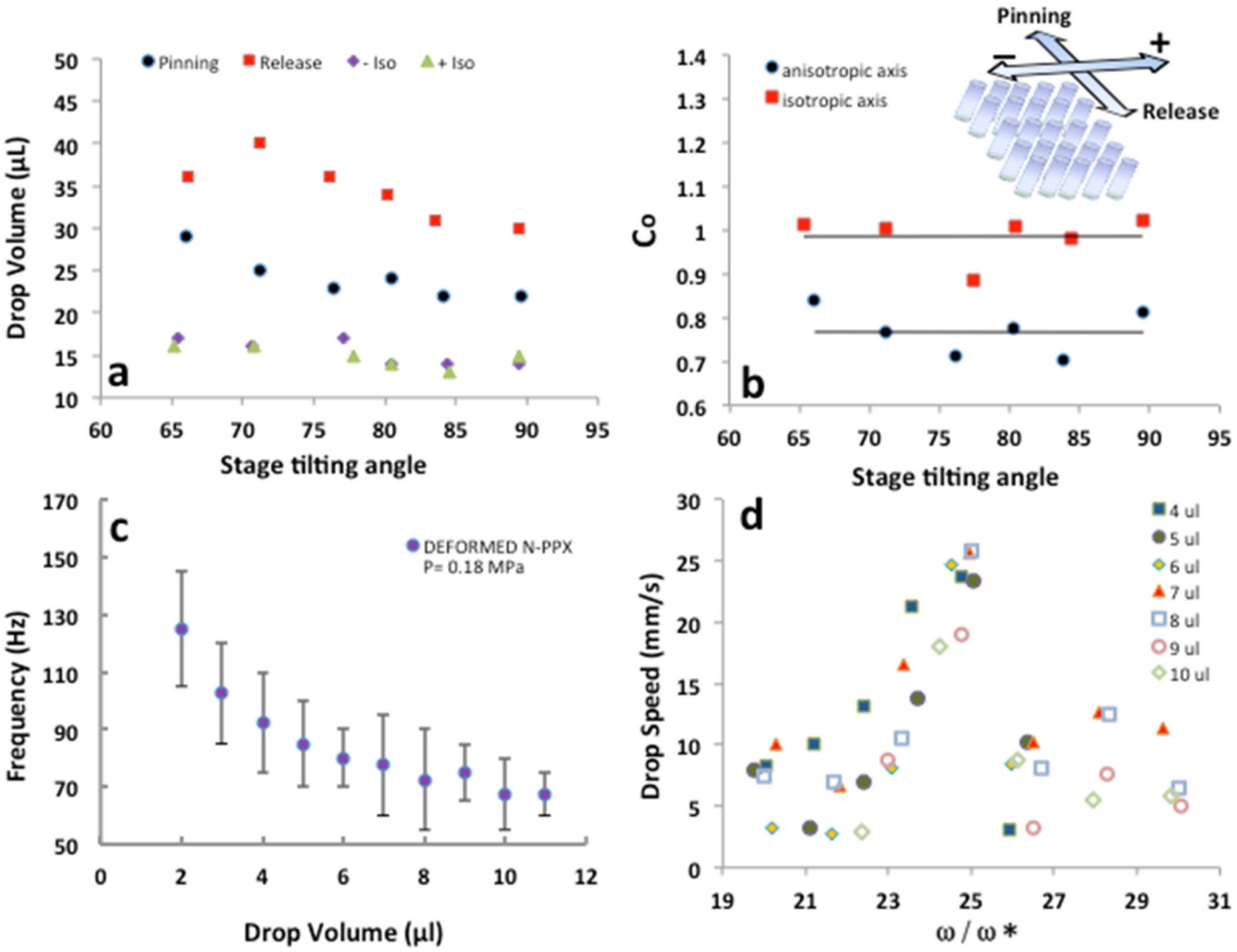

Figure 2.

(a) Critical drop volumes (**V**) as functions of the substrate tilt angles for the release ($\mathbf{V_{REL}}$), pinning ($\mathbf{V_{PIN}}$) and isotropic ($\mathbf{V_{ISO-}}$;) directions; (b) the anisotropy strength, $\mathbf{C_0}$, (*i.e.*, ratios of $\mathbf{V_{PIN}}/\mathbf{V_{REL}}$ and $\mathbf{V_{ISO-}}/\mathbf{V_{ISO+}}$) as functions of stage tilt angle is shown. Schematic of nano-PPX rods with anisotropic (pinning, release) and isotropic (+, −) directions are defined in the inset. The error bars indicate the standard deviation. (c) Vibration frequency as a function of water droplet size for deformed nanoPPX film of P = 0.18MPa (θ = 24°); (d) droplet transport speed on deformed nanoPPX film (θ = 24°) as a functional of normalized vibration frequencies shows clustering of the data around the peak velocity.

NIH-PA Author Manuscript
NIH-PA Author Manuscript
NIH-PA Author Manuscript

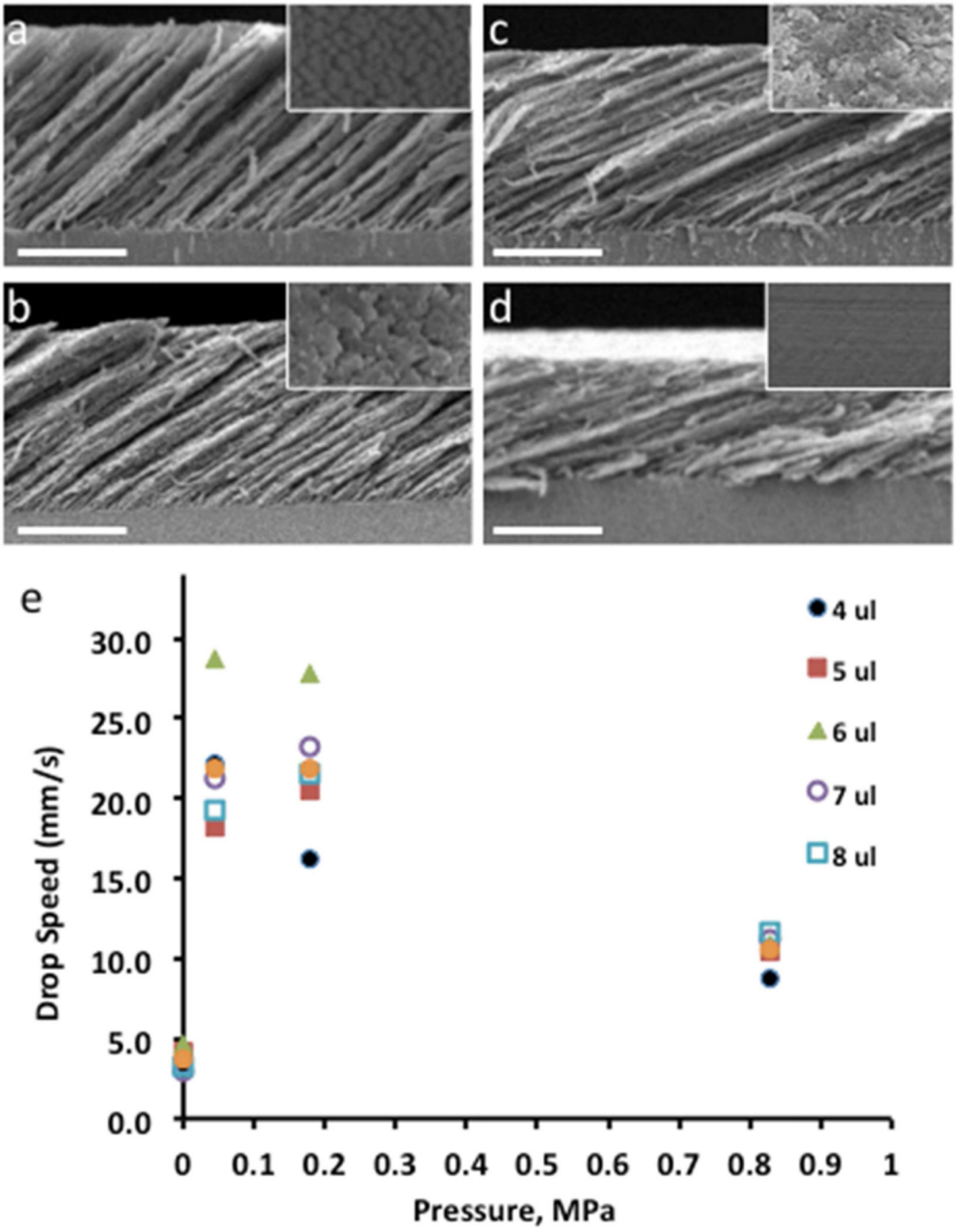

Figure 3.

Cross sectional SEM images of nano-PPX films under pressure of (a) 0 MPa (θ = 45°), (b) 0.044 MPa (θ = 32°), (c) 0.180 MPa (θ = 24°), and (d) 0.830 MPa (θ = 20°) respectively. Insets are top view SEM images of nano-PPX with roughness values of 0.29±0.1, 0.21±0.1, 0.16±0.1, 0.18±0.1 μm respectively. (e) Droplet speeds as a function of pressure on nano-PPX surfaces.

NIH-PA Author Manuscript
NIH-PA Author Manuscript
NIH-PA Author Manuscript

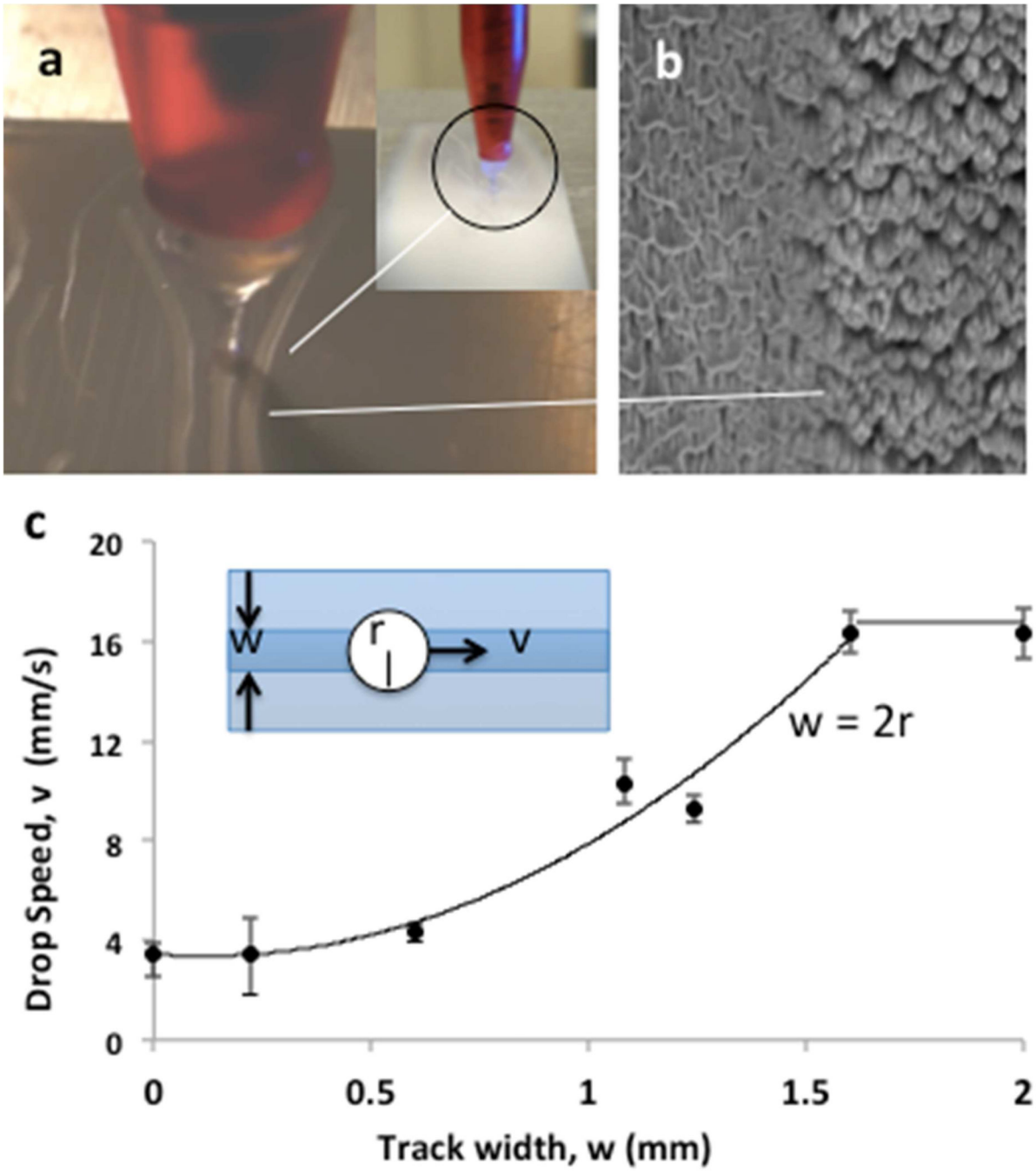

Figure 4.

(a) Close-up image of silicon tips drawing tracks (Inset: image of track drawing setup); (b) Top view SEM image of track border; (c) Drop speed dependence on track width on nano-PPX surface.

NIH-PA Author Manuscript
NIH-PA Author Manuscript
NIH-PA Author Manuscript

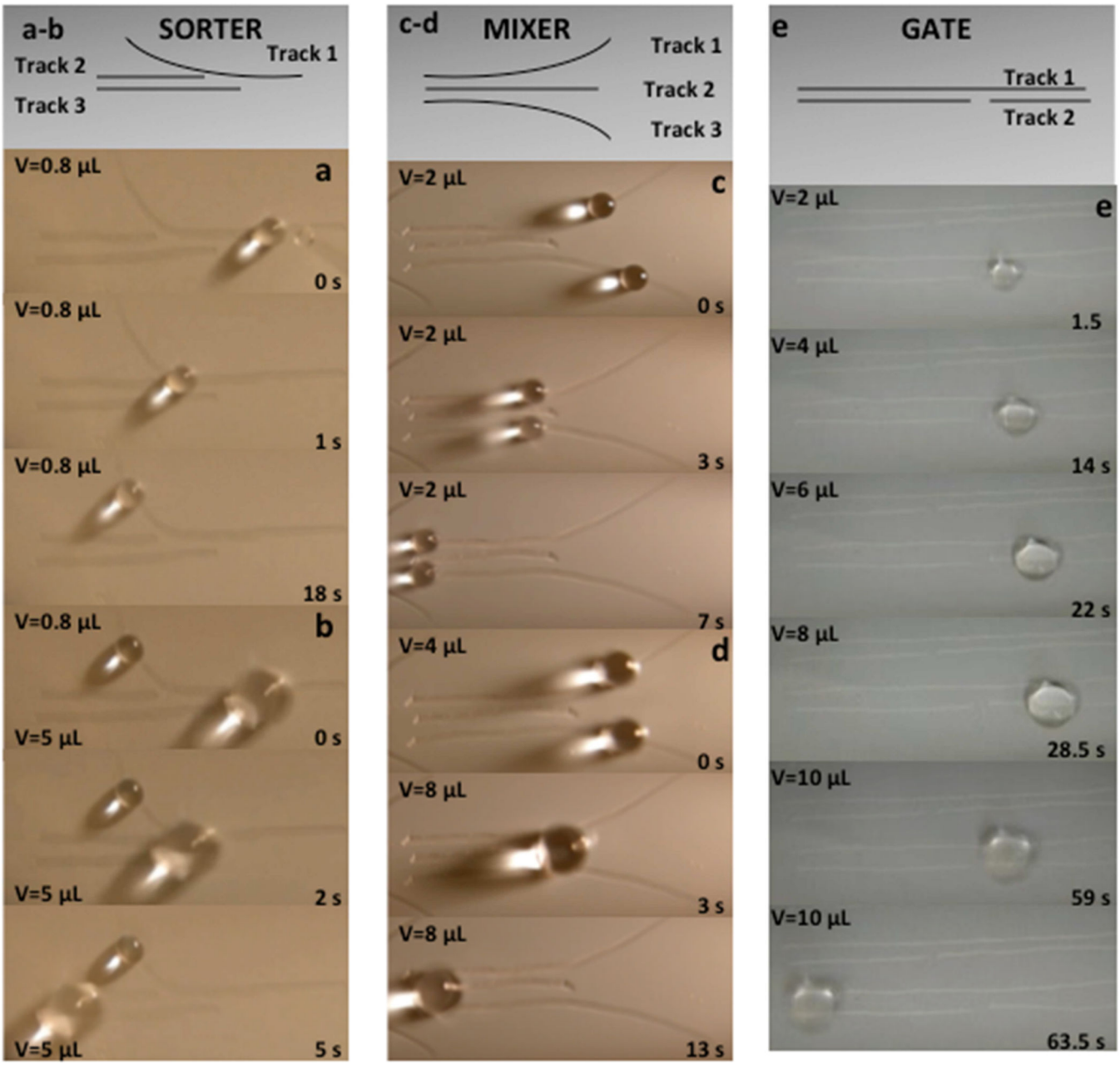

Figure 5.

(a) Volume dependent sorting; 0.8 µL droplet passes the junction towards the curved track, (b) 5 µL droplet continues straight to the double channel ahead, (c) Volume dependent mixing; 2 µL droplet moves on tracks and continues without mixing, (d) 4 µL droplet moves forward, mixes at the junction, and proceeds to the end of the channel. (e) Schematic of interrupted channel device; 2µl droplet is moving forward; 4 µl droplet (no propulsion); 6 µl droplet (no propulsion); 8 µl droplet (no propulsion); 10 µl droplet moves forward, (65 Hz frequency) jumping the gap on the tracks.